ACS APPLIED MATERIALS & INTERFACES

Research Article

www.acsami.org

Changes in Morphology and Ionic Transport Induced by ALD SiO_2 Coating of Nanoporous Alumina Membranes

Virginia Romero,[†] Víctor Vega,[‡] Javier García,[‡] Robert Zierold,[§] Kornelius Nielsch,[§] Víctor M. Prida,*[,‡] Blanca Hernando,[‡] and Juana Benavente*[,†]

[†]Departamento de Física Aplicada I, Facultad de Ciencias, Universidad de Málaga, E-29071 Málaga, Spain

[‡]Departamento de Física, Facultad de Ciencias, Universidad de Oviedo, Calvo Sotelo s/n, E-33007 Oviedo, Spain

[§]Institut für Angewandte Physik, Universität Hamburg, Jungiusstrasse 11, D-20355 Hamburg, Germany

Supporting Information

ABSTRACT: Nanoporous anodic alumina membranes (NPAMs) were produced by the two-step anodization method in sulphuric, oxalic and phosphoric acidic electrolytes displaying a hexagonally ordered spatial arrangement of pores with well controlled nanopore size distribution and low porosity. Some selected NPAMs were further modified by conformal coating their surface and inner pore walls with a thin layer of SiO_2 by means of atomic layer deposition (ALD), which reduces both the pore radii and porosity but it also seems to affect to the electric fixed charge on the membranes surface. A comparative study about the influence of silica modification of NPAMs surfaces on the ionic transport through the nanoporous membranes has been performed by measuring membrane potentials and electrochemical impedance spectroscopy with NaCl solutions. According to these results, a direct correlation between the membrane effective fixed charge and the NaCl diffusion coefficient can be established. The coating with a SiO_2 thin layer causes a reduction of 75% in the positive effective fixed charge of the NPAMs independently of their pore radii and the increase in counterion transport (cation transport number and diffusion coefficient) even through constrained nanopores, which can be of interest in several applications (microfluidics, drug delivery, nanofilter devices, etc.). Moreover, slight changes in the membrane/solution interface due to the SiO_2 cover layer are also indicated.

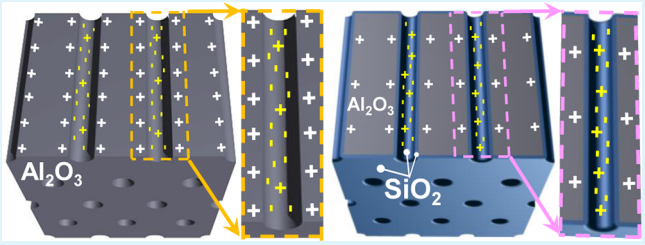

KEYWORDS: *nanoporous alumina membranes, ALD surface coating, membrane potentials, impedance spectroscopy*

1. INTRODUCTION

Nanoporous anodic alumina membranes (NPAMs) synthesized via electrochemical anodization of aluminum are formed by self-ordered structures with parallel aligned and well-defined pores keeping honeycomb structure geometry. These NPAMs have been widely employed as ordered templates for the synthesis of nanoparticles, nanotubes and nanowires,[1,2] and they are also applied in catalysis, hydrogenation, nanoelectronics and optoelectronics devices.[3−5] The excellent chemical and thermal stability of NPAMs have favored their use in separation processes, mainly when heavy metal or corrosive products are involved.[6,7] By using tubular or multichannel geometry, it is possible to overpass their fragility, which is a negative characteristic of planar and thin alumina membranes when compared with polymeric samples.[8] Furthermore, the practically ideal porous structure of NPAMs allows their use as model systems for the study of mass and ions transport trough confined channels depending on both the solute/particle size and the pore effective charge, although this latter parameter might significantly reduce the co-ion transport and significantly increase interfacial effects, e.g., concentration-polarization.[9−11] Particularly, NPAMs are employed in biosensors construction because of their relatively high surface area for the retention of enzymes or bioactive compounds.[12,13] On the one hand, their accurate nanopore diameter and narrow pore size distribution are basic requirements for the precise control of molecular transport in areas such as biosensors or biomedical (drug-delivery) applications;[14,15] but on the other hand, specific features such as surface biocompatibility or hydrophilicity may also be of importance depending on the particular application.[16−18] In order to overpass surface effects on the transport of ions or charged molecules across NPAMs, but also tuning the pore size and chemical selectivity, surface coating by adequate materials is also performed.[19−22] In this context, SiO_2 is also widely used because of its excellent thermal and chemical stability together with its outstanding biocompatibility, features that make it interesting for bio-MEMS (or biological microelectromechanical systems) applications in drug-delivery devices.[23−25]

Atomic layer deposition (ALD) is one of the most suitable techniques to perform controlled coatings of a wide range of materials over complex three-dimensional structures without

Received: October 15, 2012
Accepted: April 10, 2013
Published: April 10, 2013

shadowing effect present in many other physical or chemical deposition techniques.[26,27] Specially, in the case of NPAMs in which pore channels with aspect ratio (pore length/pore diameter) higher than 2000 need to be conformally covered, ALD can be used to modify and therefore functionalize the NPAMs surface by deposition of Al_2O_3, ZnO, or SiO_2, among others.[28,29] Hence, a combination of both, Al anodization and SiO_2 ALD deposition methods would make possible the tailor-made synthesis of complex nanostructured materials with tunable functional and biocompatible properties for applications related with transport of charged particles/molecules, such as water purification or drug-delivery devices.

Herein, we report on the fabrication of three NPAMs with different pore sizes and porosities as well as the characterization of ionic transport across them. Surface functionalization of the NPAMs with a SiO_2 protective coating by ALD allows us to get information on the effect of modification in morphology, surface pore charge and transport. Pore diameter of the studied NPAMS are around 20 nm, 35 and 165 nm, depending on the supported electrolyte and applied voltage during the anodic process, and these values are downsized after the ALD coating with a thin layer of SiO_2, thus modifying membrane morphology. Effective membrane fixed charge and its effect on ions transport through the pores of the NPAMs and NPAMs+SiO_2 modified samples are determined from membrane potential measurements performed with the membranes in contact with NaCl solutions at different concentrations. Electrochemical impedance spectroscopy measurements for a given NaCl solution were also performed as a way to check modifications in both the membrane/solution interface and the bulk membrane phase, and for independent corroboration of ionic diffusion coefficient values. The comparison between the results obtained for NPAMs and NPAMs+SiO_2 samples clearly shows the influence of the effective fixed charge on ions and salt transport through the nanoporous membranes. As a consequence of the SiO_2 thin layer coating, two different facts seem to occur: downsize of the pore dimensions and reduction of the electropositive character of the alumina surface. Finally, an increase in the diffusive transport along the contracted SiO_2 coated pores was obtained. The effect of fixed charge on the pore wall is a point of great interest when diffusion of charged species (ions, proteins, colloidal particles, etc.) is involved. This behavior added to the biocompatibility and chemical robustness provided by the SiO_2 cover may be of great interest in NPAMs applications as novel biotechnological, micronano-fluidic, and multifunctional sensing devices.[30−32]

2. EXPERIMENTAL SECTION

2.1. Membrane Fabrication. Highly ordered nanoporous alumina membranes have been fabricated by the two-step anodization process developed by Masuda et al.,[33] and explained in detail elsewhere.[34] NPAMs were synthesized through anodic processes starting from high purity Al foils (Al 99.999%), by employing different acidic aqueous solutions of sulphuric, oxalic and phosphoric acids in which, together with an appropriate selection of the anodizing voltage and electrochemical bath conditions, the pore size and the interpore distance can be modified. The characteristic parameters of the electrochemical anodization processes (kind of electrolyte and its concentration, constant anodization voltage (V_{anod}), temperature of anodization (T), and time duration of the first and second anodization processes) are collected in Table 1. The time duration of the second anodization step determines the thickness of the resulting NPAMs, which in the present work was adjusted to around 60 μm, approximately.

Table 1. Characteristic Parameters for NPAMs Fabrication

sample	fabrication procedure	V_{anod} (V)	T (°C)	$t_{first\ anod}$ (h)	$t_{second\ anod}$ (h)
Al-Ox	0.3 M oxalic anodization	40	1−3	24	24
Al-Ox +SiO_2	0.3 M oxalic anodization + ALD 5 nm SiO_2	40	1−3	24	24
Al-Sf	0.3 M sulfuric anodization	25	0−1	24	12
Al-Sf +SiO_2	0.3 M sulfuric anodization + ALD 5 nm SiO_2	25	0−1	24	12
Al-Ph	0.1 M phosphoric anodization	195	0−0.5	24	24
Al-Ph +SiO_2	0.1 M phosphoric anodization + ALD 5 nm SiO_2	195	0−0.5	24	24

After the anodization process, the remaining Al substrate was removed by wet chemical etching in a mixture of HCl and $CuCl_2$.[35] The alumina barrier layer blocking the pores bottom was removed by Reactive Ion Etching (RIE) in CF_4/O_2 plasma. This highly anisotropic etching method allows for the removal of the barrier layer without causing any noticeable increase in the pore size.[36] Some selected alumina membranes were coated with a SiO_2 thin layer of 5 nm in thickness (hereafter labeled as +SiO_2), deposited by ADL at 150 °C from 3-aminopropyltriethoxysilane (100 °C, 2 s pulse), water (20 °C, 0.5 s pulse) and ozone (RT, 2 s pulse).[37] The silica deposition was carried out in a BENEQ-TFS200 HPR system in stop-mode (45 s exposure time, 60 s pump time) to ensure homogeneous coating along the inner channels of the NPMAs.

To ensure that the thermal treatment associated with the ALD technique does not cause any structural/electrical modification of the NPAMs and, consequently, that the possible electrical modifications are associated only with the presence of the SiO_2 cover layer, we heated one specimen of the alumina samples with lower pore size at 150 °C; they will be hereafter named as Al-Ox+annealed and Al-Sf +annealed. Moreover, to distinguish between effects associated to morphological and chemical surface modification, membrane potential measurements for the Al-Sf membrane after ALD Al_2O_3 coating with the same resulting cover layer of 5 nm in thickness (sample Al-Sf +Al_2O_3) were also performed and studied.

2.2. Surface Characterization by Scanning Electron Microscopy and Contact Angle. Alumina membranes were morphologically characterized by scanning electron microscopy (SEM) top and bottom surface views and cross-section micrographs. The geometrical parameters (pore size, porosity and spatial arrangement of the nanopores) were determined by using both ImageJ and WSxM software for image analysis.[38] These samples were previously coated with a thin gold layer by means of a sputtering process to make them conductive. The SEM equipment used was a JEOL-6610LV scanning microscope, working at a voltage of 20 kV and equipped with an energy-dispersive X-ray spectrometer (EDX) INCA Energy 350-Xmax 50.

Changes in the hydrophilic character of NPAMs surface associated to the coated SiO_2 layer were determined from contact angle measurements, which were performed with a Teclis T2010 instrument equipped with a video system. Six measurements on both surfaces of each membrane were taken.

2.3. Membrane Potential and Electrochemical Impedance Spectroscopy Measurements. Membranes electrochemical characterization was performed in a dead-end test cell similar to that described in ref 10, which basically consists of two glass half-cells with the membrane placed in the middle of both cells and two magnetic stirrers in the bottom of each cell to minimize the concentration-polarization at the membrane surfaces. A Ag/AgCl reversible electrode was placed in each half-cell for electrical measurements, which were carried out with different NaCl solutions at room temperature (25 ± 2) °C, standard pH (5.8 ± 0.3) and solution stirring rates of 540 rpm.

Membrane potential ($\Delta\Phi_{mbr}$), or equilibrium electrical potential difference between two electrolyte solutions of different concentration

(c_c and c_v) at both membrane sides, was measured by connecting the electrodes to a digital voltmeter (Yokohama 7552, 1GΩ input resistance), which allows the determination of the cell potential (ΔE). Measurements were carried out by keeping constant the concentration of the solution at one side of the membrane (c_c = 0.01 M) and gradually changing the concentration of the solution at the other side (0.004 M ≤ c_v ≤ 0.1 M).[39] Both the fixed concentration value and the concentration range were selected to minimize the electric double layer thickness and to perform a significant number of membrane potential measurements (at least 14 points) under dilute solutions condition. Membranes were maintained overnight in contact with the lowest concentration solution to ensure pores filling, but it was renewed before starting the measurements. $\Delta\Phi_{mbr}$ values were obtained by subtracting the electrode potential ($\Delta\Phi_{elect}$) to the measured cell potential values, that is, $\Delta\Phi_{mbr} = \Delta E - \Delta\Phi_{elect}$.

Electrochemical impedance spectroscopy (EIS) measurements were carried out by connecting the electrodes to a Frequency Response Analyzer (FRA, Solartron 1260, England) controlled by a computer. More than 100 different frequencies in the range of 1 Hz up to 1×10^7 Hz were recorded (maximum voltage of 0.01 V) for the system electrode//0.004 M NaCl solution//membrane//0.004 M NaCl solution//electrode.[40] EIS data were corrected by software as well as the influence of connecting cables and other parasitic capacitances.

3. RESULTS AND DISCUSSION

3.1. Microstructure and Morphological Parameters of Alumina Membranes. Figure 1 shows the SEM top-view images of samples (a) Al-Ox, (b) Al-Sf, and (c) Al-Sf+SiO_2, together with (d) a SEM cross-section image of a typical Al-Ph sample, in which the inset displays an enlargement of the parallel aligned channels of the Al-Ph NPAM.

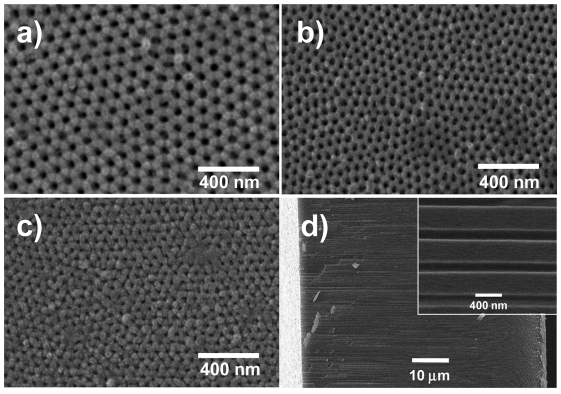

Figure 1. SEM top-view images of nanoporous alumina samples (a): Al-Ox, (b): Al-Sf, (c): Al-Sf+SiO_2; and (d): SEM cross-section image of a typical Al-Ph nanoporous alumina membrane, where the magnification in the inset shows the parallel alignment of the nanopore channels.

From the direct comparison between images b and c in Figure 1, the pore shrinkage due to the SiO_2 layer deposition can be clearly seen. Figure 2a shows the self-correlation image corresponding to Al-Ox sample shown in Figure 1a and illustrates the high spatial self-correlation (high hexagonal ordering degree) of the nanopores. The intensity profile along the line depicted in Figure 2a, which is shown in Figure 2b, allows for a precise determination of the lattice constant (i.e., the interpore distance) of the hexagonal pores arrangement.[41] This parameter is obtained from the distance between the central maximum and the adjacent second order maxima and takes a value of 105 ± 2 nm for the Al-Ox samples. The histogram displayed in Figure 2c illustrates the pore diameter

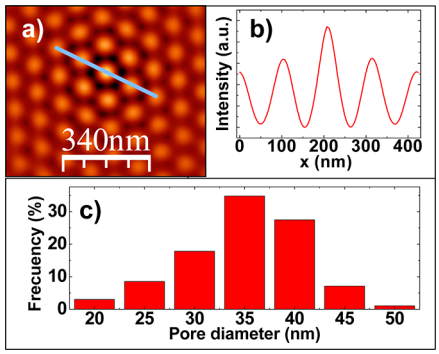

Figure 2. (a) Self-correlation from SEM top-view of the Al-Ox sample (SEM image in Figure 1a) indicating the hexagonal ordering of nanopores. (b) Profile of image (a) along the indicated line, employed for the determination of the interpore distance, D_{int}. (c) Pore size distribution corresponding to sample Al-Ox (obtained from SEM image in Figure 1a).

distribution in the same Al-Ox sample, obtained through a statistical analysis of Figure 1a. Similar studies were performed on the other NPAM samples.

Morphological surface parameters for the different samples (pore size, d_p, and interpore distance, D_{int}) as well as membrane thickness (Δx) were determined by SEM micrographs analysis and the values obtained are indicated in Table 2. Membrane

Table 2. Morphological Parameters Characteristic of the Studied NPAMs: Pore Radius ($r_p = d_p/2$), interpore distance (D_{int}), thickness (Δx), and Estimated Average Porosity ($\langle\Theta\rangle$)

sample	r_p (nm)	D_{int} (nm)	Δx (μm)	$\langle\Theta\rangle$ (%)
Al-Sf	11 ± 2	65 ± 2	51.0 ± 0.5	10
Al-Sf+SiO_2	6 ± 2	65 ± 2	51.0 ± 0.5	3
Al-Ox	16 ± 3	105 ± 2	61.0 ± 0.5	8
Al-Ox+SiO_2	11 ± 3	105 ± 2	62.0 ± 0.5	4
Al-Ph	82 ± 20	490 ± 2	66.5 ± 0.5	10
Al-Ph+SiO_2	77 ± 20	490 ± 2	66.5 ± 0.5	9

porosity (%) was determined through the expression:[42] Θ (%) = 100 $(2\pi/3^{1/2})(d_p/(2D_{int}))^2$. The estimated average porosity values ($\langle\Theta\rangle$) have been obtained by considering the porosity from both, top and bottom surface views SEM images, and the resulting values are similar but slightly smaller than those reported in the literature,[43−45] because the latter are usually obtained only from the top-surface-view SEM images and do not take into account the fact that pores generally broaden toward the film surface. According to SEM results, a reduction in pore size of approximately 45, 30, and 5% was obtained for Al-Sf+SiO_2, Al-Ox+SiO_2, and Al-Ph+SiO_2, respectively. Other surface and cross-section SEM micrographs of the studied membranes are provided as Supporting Information.

The EDX spectrum of the Al-Ox+SiO_2 sample shown in Figure 3 reveals the presence of Al, O, and Si. This later element, which corresponds to the ALD SiO_2 thin layer, supports the presence of silica covering the modified membranes surface.

This point was also clearly evident from contact angle results, which gave the following average value for original NPAMs, ϕ^{NPAM} = (64 ± 4)°, resembling to that reported by Redón et al,[46] for similar alumina membranes, whereas higher average value was obtained for the SiO_2-coated alumina samples,

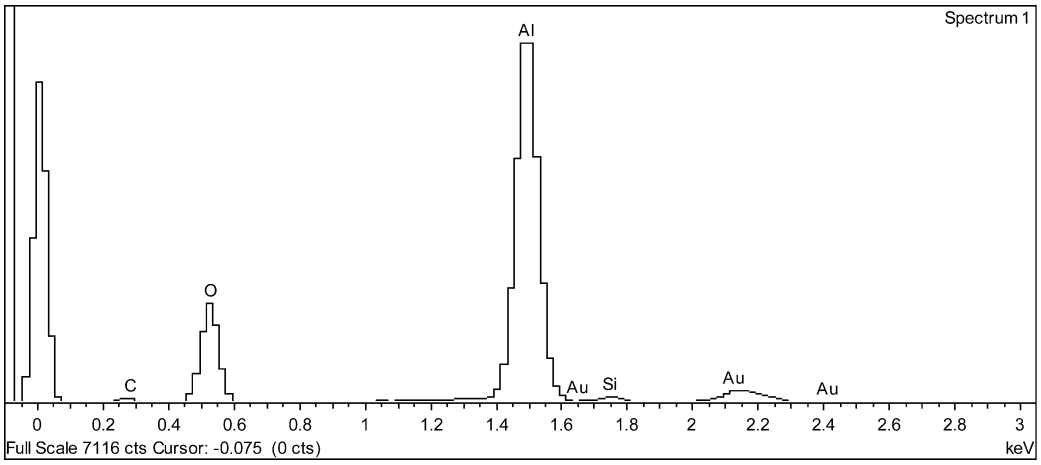

Figure 3. EDX spectrum of the Al-Ox+SiO_2 membrane indicating the presence of both aluminum and silicon oxides.

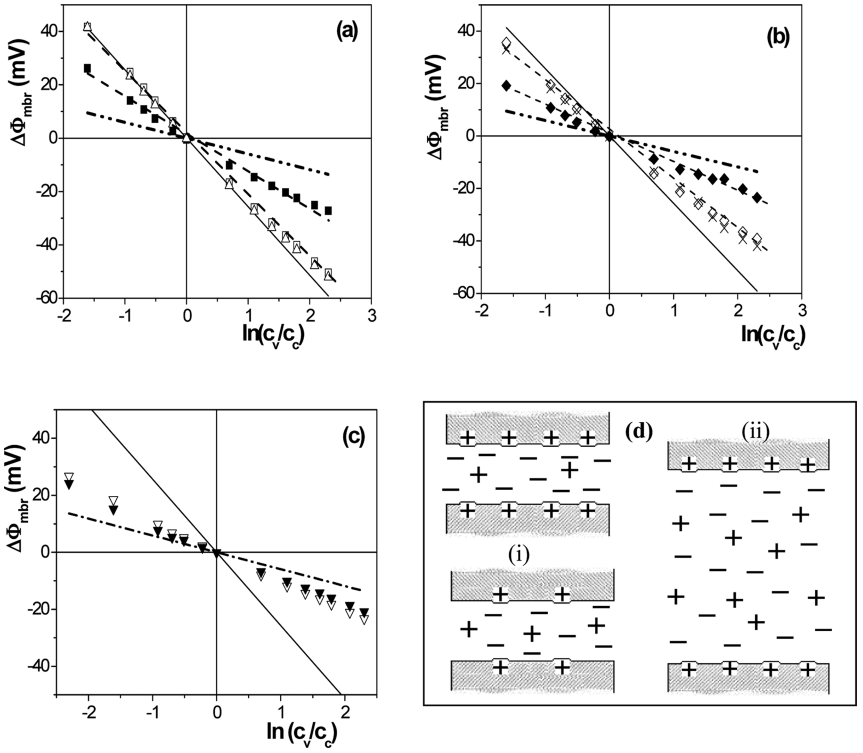

Figure 4. Membrane potential, $\Delta\Phi_{mbr}$, versus NaCl solution concentration ratio: (a) Al-Sf (□), Al-Sf+SiO_2 (■), Al-Sf+Al_2O_3 (Δ); (b) Al-Ox (◊), Al-Ox+annealed (×), Al-Ox+SiO_2 (♦); (c) Al-Ph (∇), Al-Ph+SiO_2 (▼); ideal anion-exchanger potential: solid line, NaCl solution diffusion potential: dash-dot-dot line. (d) Schematic representation of changes in pore wall charge and pore size for the membrane/electrolyte system.

$\phi^{SiO_2\text{-coated}} = (82 \pm 6)°$, in agreement with the hydrophobic character of silica. A comparison of water drop on the surface of Al-Sf and Al-Sf+SiO_2 samples is provided as Supporting Information.

3.2. Characterization of Transport Across the Nanoporous Membranes. Effective fixed charge, X_f, (charge involved in membrane-solute electrical interactions), strongly influences the transport of electrolyte solutions and/or charged species across membranes and, consequently, modifications in the charge on both external surface and pore wall (or internal surface) can affect the transport of ions. Effective fixed charge, X_f, and ion transport number, t_i, or fraction of the total current transported for one ion ($t_i = I_i/I_T$) are two significant parameters which can be determined from membrane potential values ($\Delta\Phi_{mbr}$). According to the Teorell–Meyer–Sievers or TMS theory,[47,48] membrane potential can be considered as the sum of two Donnan potentials (one at each membrane–solution interface), associated to the exclusion of the co-ions (or ions of the same sign as the membrane charge), plus a diffusion potential in the membrane due to the different mobility of the ions inside the membrane pores, that is: $\Delta\Phi_{mbr} = \Delta\phi_{Don(I)} + \Delta\phi_{dif} + \Delta\phi_{Don(II)}$. In the following expressions 1:1 electrolytes ($|z_+| = |z_-| = 1$) and diluted solutions (herein, concentrations are used instead of activities) will be considered.

The diffusion potential is given by[49]

$$\Delta\phi_{dif} = (RT/F)[(t_- - t_+)]\ln(c_c/c_v) = (RT/F)[(1 - 2t_+)]\ln(c_c/c_v) \quad (1)$$

dx.doi.org/10.1021/am400300r | ACS Appl. Mater. Interfaces 2013, 5, 3556–3564

where t_+ and t_- are the cation and anion transport numbers in the membrane, respectively. According to transport number definition, $t_+ + t_- = 1$, and for single salts: $t_- = 1 - t_+$.

The Donnan potential can be expressed as[49]

$$\Delta\phi_{Don} = (RT/F)\ln[(wX_f/2c) + [(wX_f/2c)^2 + 1)^{1/2}]] \quad (2)$$

where $w = -1$ stands for negatively charged membranes, whereas $w = +1$ represents positively charged ones. R and F correspond to the gas and Faraday constants, whereas T is the temperature of the system.

Taking into account eqs 2 and 3, the membrane potential can be expressed as[49]

$$\Delta\Phi_{mbr} = -\frac{RT}{wzF}\left[U\ln\frac{\sqrt{4y_v^2+1}+wU}{\sqrt{4y_f^2+1}+wU} - \ln\frac{c_f}{c_v}\frac{\sqrt{4y_v^2+1}+w}{\sqrt{4y_f^2+1}+w}\right] \quad (3)$$

where U is a parameter related to the ions transport numbers ($U = ((D_+ - D_-)/(D_+ + D_-) = t_+ - t_- = 2t_+ - 1$), $y_i = ((K_{S,i}c_i)/(|X_f|))$ and $K_{s,j}$ is the partition coefficient or membrane/solution concentration ratio, that is: $K_{+,i} = (\overline{c_{+,i}})/(c_i)$ and $K_{-,i} = (\overline{c_{-,i}})/(c_i)$, where the upper bar refers to the concentration inside the membrane pores. According to Dehmisch and Pusch,[50] $K_{s,j}$ can be associated with co-ion/counterion concentration at each solution/membrane side by the following expressions

$$K_{+,2} = \frac{\overline{c_{+,2}}}{c_2},\ K_{-,2} = \frac{\overline{c_{-,2}}}{c_2},\ K_{+,1} = \frac{\overline{c_{+,1}}}{c_1},\ K_{-,1} = \frac{\overline{c_{-,1}}}{c_1} \quad (4)$$

By considering the electroneutrality condition

$$w|X_f| + z_+\overline{c_+} + z_-\overline{c_-} = 0 \quad (5)$$

concentrations in the membrane can be expressed as

$$\overline{c_{-,2}} = \frac{(-w|X_f|) - (z_+\overline{c_{+,2}})}{z_-};\quad \overline{c_{-,1}} = \frac{(-w|X_f|) - (z_+\overline{c_{+,1}})}{z_-} \quad (6)$$

Figure 4 shows the membrane potential as a function of the concentration ratio for the studied membranes; for comparison, membrane potentials for an ideal anion-exchanger membrane and the solution diffusion potentials, which were determined by using $t_- = 1$ and $t_+ = t_{Na}{}^{+o}$ in eq 1, respectively, are also represented in Figure 4. Clear differences in $\Delta\Phi_{mbr}$ values between the original alumina membranes and the SiO_2 ALD-modified samples with low pore radii can be observed, whereas very similar $\Delta\Phi_{mbr}$ values were obtained for Al-Ph and Al-Ph +SiO_2 samples, which hardly differ from solution potentials. In fact, the presence of the SiO_2 coating layer on the membrane surfaces seems to reduce their barrier effect to cation movement, although these samples exhibit lower pore sizes, which might be an indication of charge reduction in the modified samples. Moreover, since ALD technique also involves a heat treatment of the samples, which might alter the structure of the NPAMs and, consequently, contribute to modification of $\Delta\Phi_{mbr}$ values, results from some nanoporous alumina samples annealed at 150 °C are shown in Figure 4b too and only small differences were obtained at high concentration ratio (around 5%). Figure 4a also shows membrane potential measurements obtained with the Al-Sf+Al_2O_3 sample and, as can be observed, $\Delta\Phi_{mbr}$ values hardly differ from those measured with the original Al-Sf membrane, which clearly established that differences in $\Delta\Phi_{mbr}$ values correspond to the SiO_2 coating layer.

The fit to eq 3 of the experimental data shown in Figure 4 allows the determination of X_f and t_+ for each membrane and the values are indicated in Table 3. According to these results

Table 3. Effective fixed charge concentration (X_f) and cation transport number (t_+) for the studied membranes

sample	X_f (M)	t_+
Al-Sf	0.020	0.143
Al-Sf+SiO_2	0.005	0.306
Al-Ox	0.010	0.224
Al-Ox+SiO_2	0.003	0.335
Al-Ph	0.002	0.340
Al-Ph+SiO_2	0.0005	0.345

the alumina membranes present positively charged surfaces, which causes a partial rejection of the Na^+ ions and, consequently, reduces the value of the cation transport number in the pores with respect to that in solution ($t_{Na}{}^{+o} = 0.385$[51]). This effect is more significant for Al-Sf and Al-Ox samples than for Al-Ph one, but the presence of the SiO_2 layer on the surface of all membranes notably reduces their effective fixed charge and, as a result of that, higher value for the cation transport number is obtained. The cation barrier effect on the transport across the different membranes, Al-Sf ≫ Al-Ox ≫ Al-Sf+SiO_2 > Al-Ox+SiO_2 > Al-Ph > Al-Ph+SiO_2, seems to be associated to the effective fixed charge more than pore size. To clarify this point, we show a scheme of the effect of both charge reduction in pores of similar size (i) and pore size increasing with similar charge (ii) in Figure 4d.

Studies of ions transport across nanofiltration membranes (pore radii ~1 nm) consider both electrical and steric/frictional effects on membrane potential and eq 3 can be modified by considering a hindrance factor ϕ ($\phi = (1 - \lambda_i)^2$, with $0 < \lambda_i < 1$),[52−54] which is included in the expression of the parameters y_i and U by means of $k_i = 6\pi/k_{i,t}$, defined as[55]

$$k_{i,t} = \frac{9}{4}\pi^2\sqrt{2}(1-\lambda_i)^{-5/2}\left[1 + \sum_{n=1}^{2} a_n(1-\lambda_i)^n\right] + \sum_{n=0}^{4} a_{n+3}\lambda^n \quad (7)$$

with $\lambda_i = r_i/r_p$, where r_p and r_i represent the membrane pore size and the Stokes radius of the ion, respectively. For a pore with cylindrical geometry, the following values for the a_j constant can be used:[53] $a_1 = -73/60$, $a_2 = 77.29/50.4$, $a_3 = -22.51$, $a_4 = -5.612$, $a_5 = -0.336$, $a_6 = -1.216$, $a_7 = 1.647$.

Figure 5(a) shows a comparison of experimental (symbols) and theoretical values (dashed lines) of membrane potential vs NaCl variable concentration for Al-Sf and Al-Ox alumina membranes, while the comparison between both SiO_2 modified samples is shown in Figure 5b. The fit of the experimental data obtained for each membrane by using the X_f and t_+ values shown in Table 3 allows the estimation of the ionic diffusion coefficients ($U = (D_+ - D_-)/(D_+ + D_-)$) and the pore radius

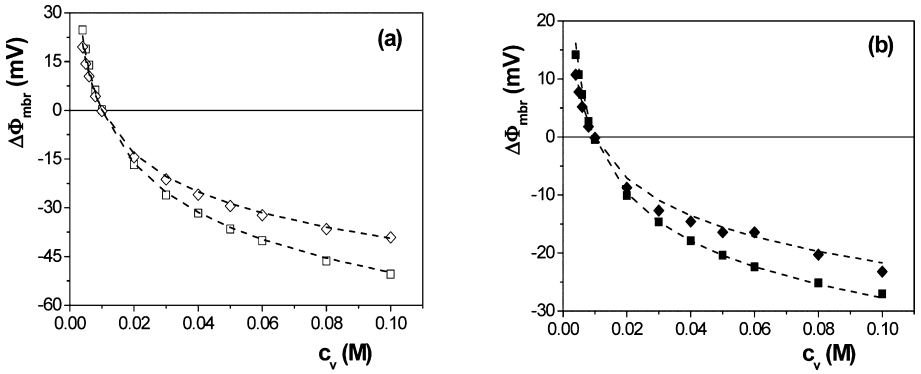

Figure 5. Comparison between experimental (symbols) and theoretical (dashed lines) membrane potential values versus NaCl variable concentration. (a) NPAMs Al-Sf (□) and Al-Ox (◊) samples; (b) ADL SiO_2-coated Al-Sf+SiO_2 (■) and Al-Ox+SiO_2 (♦) membranes.

Table 4. Cationic, Anionic, and Salt Diffusion Coefficients (D_+, D_-, D_s), Estimated Pore Radius (r_p*) and Error (ε_{pr}) Values for the Studied Membranes

sample	D_+ (m^2/s)	D_- (m^2/s)	D_s (m^2/s)	r_p* (nm)	ε_{pr} (%)
Al-Sf	2.1×10^{-10}	1.2×10^{-9}	3.4×10^{-10}	10 ± 4	4.5
Al-Sf+SiO_2	6.5×10^{-10}	1.4×10^{-9}	8.9×10^{-10}	5 ± 2	6.3
Al-Ox	3.5×10^{-10}	1.2×10^{-9}	5.4×10^{-10}	15 ± 6	4.0
Al-Ox+SiO_2	7.2×10^{-10}	1.4×10^{-9}	9.5×10^{-10}	10 ± 4	9.4
Al-Ph	8.8×10^{-10}	1.7×10^{-9}	11.5×10^{-10}	>80[a]	6.6
Al-Ph+SiO_2	7.6×10^{-10}	1.5×10^{-9}	10.1×10^{-10}	>70[a]	10.0

[a]No error reduction was observed by increasing r_p* values.

values which minimizes the error interval (ε_{pr} (%)). These results are collected in Table 4 and, as can be observed, rather good agreement between experimental and theoretical values was obtained for the studied membranes.

The analysis of the results shown in Table 4 indicates that the anion diffusion coefficient hardly depends on both effective fixed charge and pore size, but these two latter parameters clearly affect to the cation diffusion. A comparison of the values obtained for the diffusion coefficients in the membrane pores with those corresponding to aqueous solution ($D_+^\circ = 1.3 \times 10^{-9}$ m^2/s, $D_-^\circ = 2.0 \times 10^{-9}$ m^2/s, and $D_s^\circ = 1.6 \times 10^{-9}$ m^2/s)[51] shows a clear reduction in transport parameters through charged nanopores.

A similar reduction in D_{Na}+ values was already reported for a commercial NPAM with pore size and thickness similar to the Al-Sf sample,[56] but stronger reductions (around 2 orders of magnitude) have been indicated in the case of transport of macromolecules.[57] It should be remarked that all the reported results were obtained from direct diffusion measurements and analyzed on the base on Fick equation, without any explicit information on the effective pore charge as was obtained from the analysis of membrane potential measurements. In fact, a direct correlation between the effective membrane fixed charge and the salt diffusion coefficient was obtained and it is represented in Figure 6, which shows the influence of this parameter in the transport of electrolytes and charged particles.

However, it should also be pointed out that because of the type of relation between parameter U and ionic diffusion coefficients other couple of values (even with different orders of magnitude) could give the same fit, therefore the physical meaning of the process and the parameters involved have also to be considered. To ensure the adequacy of these results, we should determine ionic diffusion coefficient values from independent measurements.

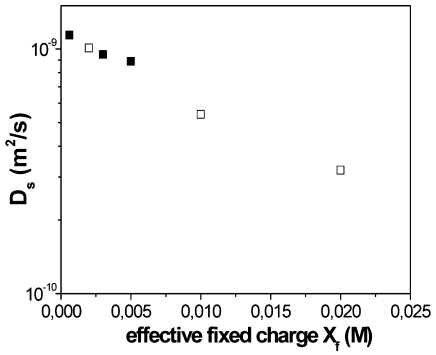

Figure 6. Salt diffusion coefficient through membranes as a function of the membrane effective fixed charge, X_f: (□) NPAM samples, (■) ALD SiO_2-coated NPAM samples.

Electrochemical impedance spectroscopy (EIS) technique was used in order to determine membrane electrical resistance by analyzing the impedance plots and using equivalent circuits as models.[40,58−60] The impedance (Z) is a complex number $Z = Z_{real} + jZ_{img}$, which can be separated into real and imaginary parts by algebra rules

$$Z_{real} = (R/[1 + (\omega RC)^2]); \quad Z_{img} = -(\omega R^2 C /[1 + (\omega RC)^2])$$

where ω represents the angular frequency ($\omega = 2\pi f$). The analysis of the impedance data is often carried out by the complex plane $Z^*(\omega)$ method using the Nyquist plot ($-Z_{img}$ vs Z_{real}). The equation for a parallel resistance-capacitance circuit (RC) gives rise to a semicircle in the $Z^*(\omega)$ plane. This semicircle has intercepts on the Z_{real} axis at high and low frequencies (that is, R_∞ for $\omega \to \infty$ and R_0 for $\omega \to 0$) being ($R_0 - R_\infty$) the resistance of the system. The maximum of the semicircle equals $0.5(R_0 - R_\infty)$ and occurs at such a frequency

dx.doi.org/10.1021/am400300r | ACS Appl. Mater. Interfaces 2013, 5, 3556−3564

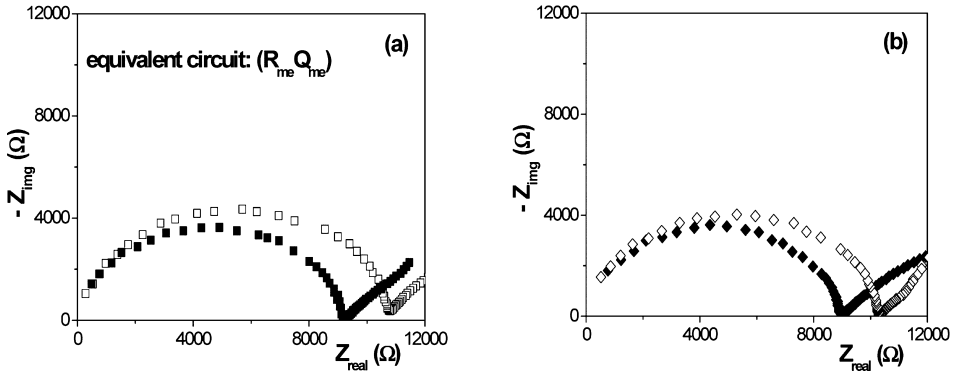

Figure 7. Nyquist plot ($-Z_{img}$ versus Z_{real}) for: (a) Al-Sf (□) and Al-Sf+SiO_2 (■) membranes; (b) Al-Ox (◊) and Al-Ox+SiO_2 (♦) membranes.

that $\omega RC = 1$, where $RC = \tau$ the relaxation time.[58] However, in the case of nonhomogeneous systems depressed semicircles as those shown in Figure 7 are obtained due to the existence of a distribution of relaxation times, and nonideal capacitors or constant phase elements (Q) are then considered. In this context, it should be indicated that, phenomenologically, the resistance represents the dissipative component of the dielectric response, whereas the capacitance describes the charge storage component of the system. More detailed explanation on EIS applied to electrolyte/membrane systems is provided as Supporting Information.

Figure 7 shows the Nyquist plot for the electrode/0.004 M NaCl solution/membrane/0.004 M NaCl solution/electrode system studied, where the plots in Figure 7a are for Al-Sf membranes, and Figure 7b shows those for Al-Ox membranes. In both cases, differences in the depressed semicircles obtained for original alumina and SiO_2 coated samples, as well as for the branches at the lowest frequencies (due to interfacial effects), can be observed. The equivalent circuit associated with the EIS diagrams corresponds to an electrical resistance (R_{me}) in parallel with a constant phase element or nonideal capacitor (Q_{me}), and the fit of the experimental data by a nonlinear program allows the estimation of both electrical parameters.[40] Because a unique relaxation process was obtained for the total system (membrane plus electrolyte solution placed between the membrane surface and the electrode), values for the membrane electrical resistance can not be determined directly but they were obtained by subtracting the electrolyte contribution (R_e, obtained from an independent measurement) to the membrane/electrolyte (R_{me}) values: $R_m = R_{me} - R_e$. However, because of the wide pore size of Al-Ph and Al-Ph+SiO_2 membranes, R_{me} and R_e values for these samples hardly differ one from each other, giving a significant error in R_m estimation, then these samples will not be considered in the following discussion.

Membrane electrical resistance is related to ionic diffusion coefficients through the following expression:[40,61] $D_+ + D_- = (RT/F^2)(\Delta x/S_m R_m)(1/c)$, where S_m is the membrane area for charge transport ($S_m = \Theta \times S_c$, and S_c the test cell area) and c the electrolyte concentration. $(D_+ + D_-)$ values obtained from EIS measurements are shown in Table 5 and compared with those obtained from D_+ and D_- values already indicated in Table 4, $(D_+ + D_-)$*. Although all the values obtained from EIS measurements are lower than those determined from membrane potential analysis, rather good agreement was achieved for both SiO_2 ALD treated membranes, that is, for the samples with lower pore size but significant lower effective charge. Taking into account this fact, an effect of charge exclusion and, consequently, differences between internal and external solution concentration might have a significant contribution in the discrepancy between both types of results.

Table 5. Comparison of Ionic Diffusion Coefficient Values Determined from Electrochemical Impedance Spectroscopy $(D_+ + D_-)$ and from Membrane Potential $(D_+ + D_-)$* Results (Table 4) for the Studied Membranes

sample	$D_+ + D_-$ (m^2/s)	$(D_+ + D_-)$* (m^2/s)
Al-Sf	0.35×10^{-9}	1.4×10^{-9}
Al-Sf+SiO_2	1.22×10^{-9}	2.0×10^{-9}
Al-Ox	0.88×10^{-9}	1.5×10^{-9}
Al-Ox+SiO_2	1.36×10^{-9}	2.1×10^{-9}

Impedance diagrams can also give qualitative information on interfacial effects.[39,57] Figure 8 shows a comparison of the Bode plots (Z_{real} versus frequency or $-Z_{img}$ versus frequency) for Al-Ox and Al-Ox+SiO_2 samples, where bulk (f > 1 kHz) and interface (f < 1 kHz) differences in the real (Figure 8a) and imaginary (Figure 8b) parts of the impedance function can separately be observed.

According to these diagrams the real part of the impedance (associated to the transport of charge) presents clear bulk differences, but similar values are obtained for the imaginary part (related to charge storage); however, interfacial effects are significant in both impedance contributions, which seems to agree with the SiO_2 coating of the external surface of the alumina membrane already determined from contact angle measurements.

■ CONCLUSIONS

NPAMs with controlled morphologies have been successfully produced by the two-step anodization method and ALD coated with a SiO_2 thin layer that replicates their morphology conformally covering their surfaces. Our comparative studies on the microstructure together with the transport properties obtained for both the original alumina and the SiO_2-coated NPAMs reveal that the ALD coating is an efficient method to modify both the nanoporous membrane morphology and its effective surface charge and, consequently, the transport parameters in the case of electrolyte solutions or charged species through the membrane nanopores. In fact, a reduction of 75% in the NPAM effective fixed charge as a result of the ALD SiO_2 coating was obtained independently of the membrane pore radii. Additionally, no structural changes related with the thermal treatment associated to ALD modification were observed, whereas the pore reduction associated to the Al_2O_3 ALD coating does not seem to cause

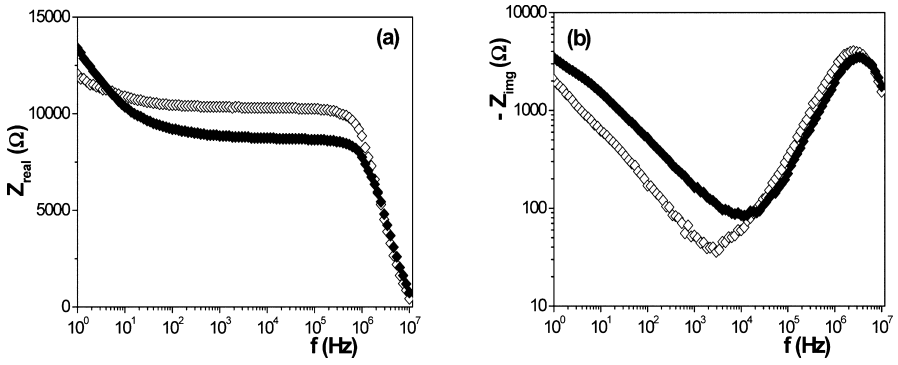

Figure 8. Bode plots: (a) Z_{real} versus frequency; (b) $-Z_{img}$ versus frequency, for Al-Ox (◊) and Al-Ox+SiO_2 (♦) membranes.

a significant modification in the ionic transport and, consequently, membrane selectivity.

SiO_2 ALD-coated modification may enable novel applications of NPAMs as nanofiltration devices and microfluidics or other biotechnological related applications due to the enhancement of their specific properties and chemical robustness added by the SiO_2 cover layer as well as pore size reduction, but it also reduces the selectivity of the membranes to co-ions.

■ ASSOCIATED CONTENT

Supporting Information

Extensive SEM top-view and cross-section micrographs of the obtained NPAMs as well of those of the state-of-the-art NPAMs after being ALD covered. Contact angle measurements of some selected samples in the as-obtained state and after being ALD coated. Electrochemical impedance spectroscopy (EIS) analysis (Nyquist and Bode plots), for an electrolyte and electrolyte/NPAMs systems depending on membranes features: symmetric (dense and porous) and asymmetric. Some selected references related to the use of EIS for the determination of membrane conductivity, not included in the reference section. This material is available free of charge via the Internet at http://pubs.acs.org/.

■ AUTHOR INFORMATION

Corresponding Author

*E-mail: vmpp@uniovi.es (V.M.P.); j_benavente@uma.es (J.B.).

Notes

The authors declare no competing financial interest.

■ ACKNOWLEDGMENTS

The authors thank MINECO (Project CTQ2011-27770 FEDER funds) and MICINN (projects MAT2009-13108-C02-01 and MAT2010-20798-C05-04) for financial support. V. Romero also thanks to CICYT for her FPU grant, while J. Garcia thanks to FICyT by his Severo Ochoa grant. The scientific support from the SCT's of the University of Oviedo (Nanoporous Membranes Laboratory and Electronic Microscopy units) is also acknowledged. Further financial support for R. Zierold was provided by the state of Hamburg through the Excellence Clusters "Nanotechnology for Medicine" as well as by the DFG projects DFG-NI 616/12-2 and 616/18-1.

■ REFERENCES

(1) Sulka, G. D. Chapter 1: Highly Ordered Anodic Porous Alumina Formation by Self-Organized Anodizing. In *Nanostructured Materials in Electrochemistry*; Eftekhari, A., Ed.; Wiley−VCH: Weinheim, Germany, 2008; pp 1−116.

(2) Oliveira, C. P.; Freitas, R. G.; Mattoso, L. H. C.; Pereira, E. C. Chapter 2: Nanostructured Materials Synthesized Using Electrochemical Techniques. In *Nanostructured Materials in Electrochemistry*; Eftekhari, A., Ed.; Wiley−VCH: Weinheim, Germany, 2008; pp 117−186.

(3) Kormann, H.-P; Schmid, G.; Pelzer, K.; Philippot, K.; Chaudret, B. *Z. Anorg. Allg. Chem.* **2004**, *630*, 1913−1918.

(4) Sato, A.; Pennec, Y.; Shingne, N.; Thurn-Albrecht, T.; Knoll, W.; Steinhart, M.; Djafari-Rouhani, B.; Fytas, G. *ACS Nano* **2010**, *4*, 3471−3481.

(5) Gonzalez Díaz, B.; Garcia-Martin, A.; Armelles, G.; Navas, D.; Vázquez, M.; Nielsch, K.; Wehrspohn, R. B.; Gösele, U. *Adv. Mater.* **2007**, *19*, 2643−2647.

(6) Bhave, R. R. In *Inorganic Membranes: Synthesis, Characterization and Application*; Bhave, R. R., Ed.; Van Nostrand Reinhold: New York, 1991; pp 64−94.

(7) Wang, X. H.; Li, C. Y.; Chen, G.; He, L.; Cao, H. *Appl. Phys. A: Mater. Sci. Process.* **2010**, *98*, 745−749.

(8) Mulder, M. In *Basic Principles of Membrane Technology*; Kluwer Academic: Dordrecht, The Netherlands, 1991; pp 281−288.

(9) Helfferich, F. In *Ion Exchange*; McGraw-Hill: New York, 1962; pp 339−420.

(10) Sollner, K. *J. Macromol. Sci.−Chem.* **1969**, *3*, 1−86.

(11) Pelaez, L.; Vázquez, M. I.; Benavente. *Ceram. Int.* **2010**, *36*, 797−801.

(12) Darder, M.; Aranda, P.; Hernández-Vélez, M.; Manova, E.; Ruiz-Hitzky, E. *Thin Solid Films* **2006**, *495*, 321−326.

(13) Alvarez, S. D.; Li, C.-P.; Chiang, C. E.; Schuller, I. K.; Sailor, M. J. *ACS Nano* **2009**, *3*, 3301−3307.

(14) Mo, Y.; Fei, T. *Nano LIFE* **2012**, *2*, 1230003.

(15) Adigal, S. P.; Jin, Ch.; Curtis, L. A.; Monteiro-Riviere, N. A.; Narayan, R. J. *WIREs Nanomedicine and Nanobiotechnology*; Wiley: New York, 2009; Vol. *1*, pp 568−581.

(16) Wolfrum, B.; Mourzina, Y.; Sommerhage, F.; Offenhäusser, A. *Nano Lett.* **2006**, *6*, 453−457.

(17) Li, Z.; Wang, J.; Zhang, Y.; Wang, J.; Jiang, L.; Song, Y. *Appl. Phys. Lett.* **2010**, *97*, 233107.

(18) Mateo, J. N.; Kulkarni, S. S.; Das, L.; Bandyopadhyay, S.; Tepper, G. C.; Wynne, K. J.; Bandyopadhyay, S. *Nanotechnology* **2011**, *22*, 035703.

(19) Szczepanski, V.; Vlassiouk, I.; Smirnov, S. *J. Membr. Sci.* **2006**, *281*, 587−591.

(20) Penumetcha, S. S.; Kona, R.; Hardin, J. L.; Molder, A. L.; Steinle, E. D. *Sensors* **2007**, *7*, 2942−2952.

(21) Losic, D.; Cole, M. A.; Dollmann, B.; Vasilev, K.; Griesser, H. J. *Nanotechnology* **2008**, *19*, 245704.

(22) Velleman, L.; Triani, G.; Evans, P. J.; Shapter, J. G.; Losic, D. *Microporous Mesoporous Mater.* **2009**, *126*, 87−84.

(23) Lu, J.; Liong, M.; Li, Z.; Zink, J. I.; Tamanoi, F. *Small* **2010**, *6*, 1794−1805.

(24) Ruiz-Hernández, E.; Baeza, A.; Vallet-Regí, M. *ACS Nano* **2011**, *5*, 1259−1266.
(25) Finch, D. S.; Oreskovic, T.; Ramadurai, K.; Herrmann, C. F.; George, S. M.; Mahajan, R. L. *J. Biomed. Mater. Res.* **2008**, *87A*, 100−106.
(26) Trewyn, B. G.; Nieweg, J. A.; Zhao, Y.; Lin, V. S.-Y. *Chem. Eng. J.* **2008**, *137*, 23−29.
(27) George, S. M. *Chem. Rev.* **2010**, *110*, 111−131.
(28) Bae, C.; Shin, H.; Nielsch, K. *MRS Bull.* **2011**, *36*, 887−897.
(29) Hiller, D.; Zierold, R.; Bachmann, J.; Alexe, M.; Yang, Y.; Gerlach, J. W.; Stesmans, A.; Jivanescu, M.; Müller, U.; Vogt, J.; Hilmer, H.; Löper, P.; Künle, M.; Munnik, F.; Nielsch, K.; Zacharias, M. *J. Appl. Phys.* **2010**, *107*, 064314.
(30) Lee, S. B.; Mitchell, D. T.; Trofin, L.; Nevanen, T. K.; Söderlund, H.; Martin, C. R. *Science* **2002**, *296*, 2198−2200.
(31) Fan, R.; Karnik, R.; Yue, M.; Li, D.; Majumdar, A.; Yang, P. *Nano Lett.* **2005**, *5*, 1633−1637.
(32) Moreno i Codinachs, L.; Birkenstock, C.; Garma, T.; Zierold, R.; Bachmann, J.; Nielsch, K.; Schöning, M. J.; Fontcuberta i Morral, A. *Phys. Status Solidi A* **2009**, *206*, 435−441.
(33) Masuda, H.; Fukuda, K. *Science* **1995**, *268*, 1466−1468.
(34) Romero, V.; Vega, V.; García, J.; Prida, V. M.; Hernando, B.; Benavente, J. *J. Colloid Interface Sci.* **2012**, *376*, 40−46.
(35) Xu, T. T.; Piner, R. D.; Ruoff, R. S. *Langmuir* **2003**, *19*, 1443−1445.
(36) Liang, J.; Chik, H.; Yin, A.; Xu, J. *J. Appl. Phys.* **2002**, *91*, 2544−2546.
(37) Bachmann, J.; Zierold, R.; Chong, Y. T.; Hauert, R.; Sturm, C.; Schmidt-Grund, R.; Rheinländer, B.; Grundmann, M.; Gösele, U.; Nielsch, K. *Angew. Chem., Int. Ed.* **2008**, *120*, 6272−6274.
(38) Horcas, I.; Fernandez, R.; Gomez-Rodriguez, J. M.; Colchero, J.; Gomez-Herrero, J.; Baro, A. M. *Rev. Sci. Instrum.* **2007**, *78*, 013705.
(39) Benavente, J. Chapter 9: Characterization Electrical Characterization of Membranes. In *Monitoring and Visualizing Membrane-Based Process, Part II: Electrical, Laser and Acoustic Techniques for Membrane Process*; Güell, C., Ferrando, M., López, F., Eds.; Wiley−VCH: Weinheim, Germany, 2009; pp 177−207.
(40) Benavente, J. Chapter 2: Use of Impedance Spectroscopy for Characterization of Modified Membranes. In *Membrane Modification: Technology and Applications*; Hilal, N., Khayet, M., Wright, C. J., Eds.; CRC Press: Boca Raton, FL, 2012; pp 21−40.
(41) Mínguez-Bacho, I.; Rodríguez-López, S.; Asenjo, A.; Vázquez, M.; Hernández-Vélez, M. *Appl. Phys. A: Mater. Sci. Process.* **2012**, *106*, 105−112.
(42) Nielsch, K.; Choi, J.; Schwirn, K.; Wherspohn, R. B.; Gösele, U. *Nano Lett.* **2002**, *2*, 677−680.
(43) Patermarakis, G.; Masavetas, K. *J. Electroanal. Chem.* **2006**, *588*, 179−189.
(44) Prida, V. M.; Pirota, K. R.; Navas, D.; Asenjo, A.; Hernández-Vélez, M.; Vázquez, M. *J. Nanosci. Nanotechnol.* **2007**, *7*, 272−285.
(45) Chen, W.; Wu, J.-S.; Xia, X.-H. *ACS Nano* **2008**, *2*, 959−965.
(46) Redón, R.; Vázquez-Olmos, A.; Mata-Zamora, M. E.; Ordoñez-Medrano, A.; Rivera-Torres, F.; Saniger, J. M. *Rev. Adv. Mater. Sci.* **2006**, *11*, 79−87.
(47) Meyer, K. H.; Sievers, J. F. *Helv. Chim. Acta* **1936**, *19*, 646−651.
(48) Teorell, T. *Discuss. Faraday Soc.* **1956**, *21*, 9−26.
(49) Lakshminarayanaiah, N. In *Transport Phenomena in Membranes*; Academic Press: New York, 1969; pp 195−205.
(50) Dehmisch, H.-U.; Pusch, W. *J. Colloid Interface Sci.* **1972**, *69*, 247−261.
(51) Robinson, R. A.; Stokes, R. H. In *Electrolyte Solutions*; Butterworth & Co..: London, 1959; pp 284−335.
(52) Szymczyk, A.; Fievet, P. *J. Membr. Sci.* **2005**, *252*, 77−88.
(53) Lanteri, Y.; Szymczyk, A.; Fievet, P. *Langmuir* **2008**, *24*, 7955−7962.
(54) Benavente, J.; Silva, V.; Pradanos, P.; Palacio, L.; Hernandez, A.; Jonsson, G. E. *Langmuir* **2010**, *26*, 11841−11849.
(55) Deen, W. M. *AIChE J.* **1987**, *33*, 1409−1425.
(56) Bluhm, E. A.; Schroeder, N. C.; Bauer, E.; Fife, J. N.; Chamberlin, R. M.; Abney, K. D.; Young, J. S.; Jarvinen, G. D. *Langmuir* **2000**, *16*, 7056−7060.
(57) Kennard, R.; de Sisto, W. J.; Mason, M. D. *Appl. Phys. Lett.* **2010**, *97*, 213701.
(58) Macdonald, J. R.; Kenan, W. R. In *Impedance Spectroscopy: Emphasizing Solid Materials and Systems*; Macdonald, J. R., Ed.; John Wiley & Sons: New York, 1987; pp 12−26.
(59) Asaka, A. *J. Membr. Sci.* **1990**, *50*, 71.
(60) Escobar, C. A.; Zulkifli, A. R.; Faulkner, C. J.; Trzeciak, A.; Jennings, G. K. *ACS Appl. Mater. Interfaces* **2012**, *4*, 906.
(61) Benavente, J.; García, J. M.; de la Campa, J. G.; de Abajo, J. *J. Membr. Sci.* **1996**, *114*, 51−57.